Identification of Sympathetic Nervous System Activation from Skin Conductance: A Sparse Decomposition Approach with Physiological Priors

Md. Rafiul Amin, Student Member, IEEE, and Rose T. Faghih, Member, IEEE,

Abstract— Objective: Sweat secretions lead to variations in skin conductance (SC) signal. The relatively fast variation of SC, called the phasic component, reflects sympathetic nervous system activity. The slow variation related to thermoregulation and general arousal is known as the tonic component. It is challenging to decompose the SC signal into its constituents to decipher the encoded neural information related to emotional arousal. Methods: We model the phasic component using a second-order differential equation representing the diffusion and evaporation processes of sweating. We include a sparse impulsive neural signal that stimulates the sweat glands for sweat production. We model the tonic component with several cubic B-spline functions. We formulate an optimization problem with physiological priors on system parameters, a sparsity prior on the neural stimuli, and a smoothness prior on the tonic component. Finally, we employ a generalized-crossvalidation-based coordinate descent approach to balance among the smoothness of the tonic component, the sparsity of the neural stimuli, and the residual. Results: We illustrate that we can successfully recover the unknowns separating both tonic and phasic components from both experimental and simulated data (with $R^2 > 0.95$). Further, we successfully demonstrate our ability to automatically identify the sparsity level for the neural stimuli and the smoothness level for the tonic component. Conclusion: Our generalized-cross-validation-based novel method for SC signal decomposition successfully addresses previous challenges and retrieves a physiologically plausible solution. Significance: Accurate decomposition of SC could potentially improve cognitive stress tracking in patients with mental disorders.

Index Terms—Biomedical signal processing, deconvolution, optimization, sparse recovery, state-space methods, system identification

I. INTRODUCTION

This paper was presented in part at the proceedings of the IEEE Engineering in Medicine and Biology Society Conference [1]. This work was supported in part by NSF grant 1942585 - CAREER: MIND-WATCH: Multimodal Intelligent Noninvasive brain state Decoder for Wearable AdapTive Closed-loop arcHitectures and 1755780 - CRII: CPS: Wearable-Machine Interface Architectures. Rose T. Faghih served as the senior author.

Md. Rafiul Amin and Rose T. Faghih are with the Department of Electrical and Computer Engineering at the University of Houston, Houston, TX 77004 USA (e-mail: {mamin, rtfaghih}@uh.edu). Correspondence should be addressed to senior author Rose T. Faghih.

LTHOUGH the skin's electrical activity was first ob-A served in the 1880s, the term "electrodermal activity" (EDA) was first introduced in 1966 as a common phrase for electrical phenomena in the skin [1], [2]. Since its discovery, EDA has been very popular in psychophysiology research as variations in the skin's electrical conductivity correlate with the sympathetic nervous system (SNS) activation. SNS is a part of our body's autonomic nervous system (ANS), which is primarily responsible for the fight-or-flight response mechanism. EDA can be exosomatically recorded by measuring skin conductance (SC). Some authors use the term "galvanic skin response" (GSR) to refer to the SC. In response to emotional stress, ANS stimulates sweat glands depending on the psychological and physiological demands. Consequently, salty secretions from sweat glands increase the SC. SC measurements can be analyzed to investigate the corresponding ANS activation, which contains a great deal of information about human emotional arousal [3].

SC is considered as a composition of two components [2], [4]–[7]. The relatively slow varying component, called the tonic component, is generally related to the thermoregulation of the body, ambient temperature, humidity, and the general arousal of a person [2], [8]. Wickramasuriya et al. [9] showed that the tonic component can be incorporated in an arousal state estimation scheme assuming it contains the general arousal information of a person. Some authors have measured it as SC level (SCL) [2]. On the contrary, the comparatively fast varying component is a reflection of neural stimulation from the SNS. The fast varying component is called the phasic component which is comprised of discrete SC responses (SCRs). Discrete SCRs can be related to various SNS activation events. In summary, SC can be represented as the sum of two convolution operations: (1) between a sparse neural stimuli from SNS and a fast physiological smoothing kernel and (2) between some arbitrary unknown activation function and a slow physiological smoothing kernel. There is a growing interest in identifying such systems as well as the underlying neural stimuli representation SNS activation for a better understanding of physiological phenomena [10], [11].

Appropriate EDA analysis along with SNS activation identification technique has applications in a wide range of fields such as mental disorders, pain, cognitive stress tracking,

wakefulness, etc. As different physiological signals, including SC, contain information about someone's emotional arousal, they have potential applications in the field of mental health. For example, preventing deaths from mental disorders with regular tracking could be one potential application as Walker et al. [12] reported that a large portion of the deaths worldwide is attributable to mental health-related disorders. A metaanalysis shows that mental disorders are a major risk factor for suicide [13]. Suicide is one of the leading causes of death in the United States in the year 2017, and it has increased by 3.7% from the previous year [14]. Suicide related costs for the United States were \$93.5 billion in 2013 alone [15]. Shepard et al. [15] emphasized the community based immediate psychiatric services, including telepsychiatric support for reducing suicide-related costs. Regular tracking of problematic patterns of emotional regulation could potentially help prevent psychiatric disorders [16]. Electroencephalogram, electrocardiogram, respiration, functional near-infrared spectroscopy [17], and EDA, could be investigated to identify abnormal patterns of emotional regulation [18]. Day to day tracking and analysis of emotional regulation requires reliable wearable implementations for suicide-prone patients.

In a different context, studies have also shown that abnormal SC recordings can be attributed to diabetic neuropathy and other diabetic diseases [19]-[21]. Diabetic neuropathy refers to the small nerve damages caused by prolonged exposure to high levels of blood glucose concentration [22]. Small nerves in the legs, feet, and hands are more prone to neuropathy [22]. The small nerve fibers also include the sudomotor nerves that are primarily responsible for delivering the SNS activation to the sweat glands for sweat secretion. Abnormal SC variation or asymmetry of SC recordings from different skin regions might be an indication of diabetic neuropathy. According to clinical diagnostics, the development of early stages of sweat formation disorders is related to various forms of illnesses, including hypohidrosis or anhidrosis, which accompany diseases like diabetes mellitus [23]. Systematic analysis of SC recording to identify these asymmetries can be crucial for the early prevention of such illness.

In the early days, most of the SC studies in psychophysiology were performed with only basic statistics. In the last two decades, researchers have come up with systematic analysis tools with a goal of understanding SNS activation patterns [24]. Several popular methods have been widely used for decomposing SC recording into its constituents. Benedek et al. [5], [6] proposed two methods within a toolbox named LedaLab to decompose SC signal into several discrete SCRs. However, their methods lead to non-sparse solutions for neural stimuli which may over-fit to the noise. Bach et al. [25] have proposed the dynamic causal modeling (DCM) approach for inferring the neural stimuli. They have considered a linear time-invariant system for modeling SCRs. They optimize the model parameters for a large dataset. They later also proposed a matching pursuit (MP) approach for alternative and faster implementation [26]. However, as a pre-processing step, they perform band-pass filtering (between 0.015 and 5 Hz) to remove the tonic component [27]. As both phasic and tonic components are SC measures, they are non-negative and both

should have a spectral overlap in the low-frequency region. Therefore, simple band-pass filtering introduces physiologically impossible negative values in the filtered signal and hence can distort the actual underlying components. Greco et al. [7] proposed a decomposition algorithm based on quadratic programming named cvxEDA where they have considered two different dictionaries for modeling tonic and phasic components. They considered the sparsity condition in neural stimuli. Nonetheless, the manual selection of the SCR shape parameters as well as the hyperparameters for imposing the sparsity prior on SNS activity and smoothness prior on the tonic component makes it challenging to find an appropriate solution. Hernando-Gallego et al. [28] proposed a fast and sparse decomposition algorithm named sparsEDA, however, it seems to provide an overly sparse solution leading to missing significant SCRs. Studies in [29]–[32] proposed coordinate descent deconvolution approaches to account for the individual differences in the SCR shape parameters, but these do not solve for the tonic component.

In the present study, we propose an algorithm to recover the SNS neural stimuli, the underlying SCR shape parameters, and the tonic component from observed SC sampled data. Inspired by the works in [7], [29], [33]–[38], we use a second-order differential equation model based on diffusion and evaporation process of sweat to relate SC to the internal unobserved neural stimuli and model the tonic component with a set of cubic basis-spline (B-spline) functions. We formulate an optimization problem based on the proposed model including: 1) Gaussian prior on SCR shape parameters, 2) sparsity prior on neural stimuli (l_1 -norm penalization), and 3) smoothness prior on the tonic component (energy penalization, i.e. l_2 -norm penalization on the cubic B-spline coefficients). We propose a block coordinate descent approach to recover the unknowns by incorporating sparse recovery for the neural stimuli and the interior-point method for the SCR shape parameters and the tonic component estimation. Moreover, we implement generalized-cross-validation (GCV) to obtain regularization parameters for both the l_1 -norm and l_2 -norm penalization terms, respectively for the neural stimuli and cubic B-spline coefficients. Finally, we analyze both experimental and simulated SC datasets to show the performance of our proposed approach.

II. METHOD

A. Dataset Description

In this study, we analyse the SCRs to loud sounds [39], auditory oddballs [40], pain by electric shocks [41], white noise bursts [42], visual detection tasks [43]. The experiments were designed to investigate and model event-related SCRs [44]. The number of participants, gender, and age information is provided in Table I. Dataset 1 contains three-channel SC data (SC measurement from the thenar/hypothenar of the non-dominant hand, the middle phalanx of the dominant second and third finger, and the medial plantar surface of the non-dominant foot) of each of the 26 participants. The rest of the datasets collect data only from the thenar/hypothenar of the non-dominant hand. Therefore, we use the SC recordings

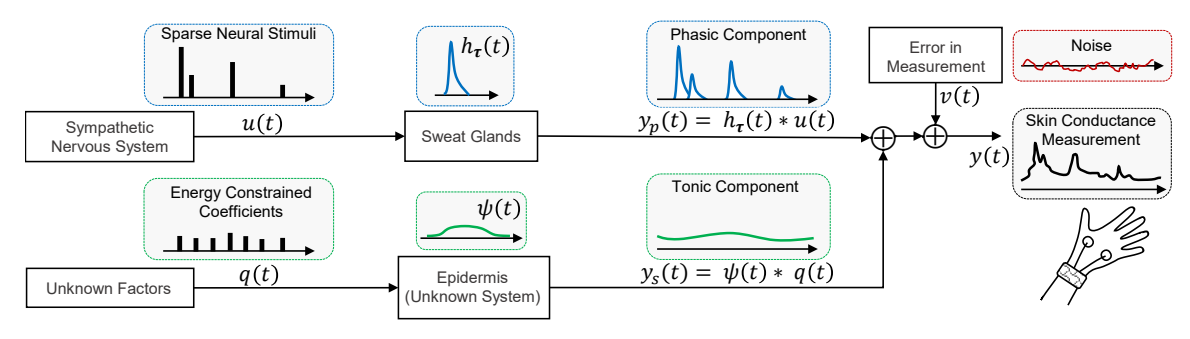


Fig. 1. **Model Block Diagram.** A single neural stimuli signal u(t) generated by the SNS is responsible for the SCR in a particular skin region of the body. The block diagram shows the neural stimuli u(t) convolving with sweat glands in a particular region of the skin having a phasic response function $h_{\tau}(t)$ to generate phasic component. The tonic component is represented as a convolution between a signal representing the weights in different time instances for the q(t) and a function $\psi(t)$ denoting the smooth variation. $\nu(t)$ represents the measurement error.

TABLE I
SUMMARY OF DATASETS USED IN THE STUDY

Dataset	Experiment	Number of	A 00 (1100mg)
No.	Туре	Participants	Age (years)
1	Loud Sound Stimulation	26 (13 M, 13 F)	24.4+/-4.9
2	Auditory Oddball Task	20 (9 M, 11 F)	21.8+/-3.3
3	Pain by Electric Shocks	19 (9 M, 10 F)	21.8+/-3.3
4	White Noise Stimulation	22 (11 M, 11 F)	24.7+/-4.5
5	Visual Detection Task	22 (11 M, 11 F)	24.7+/-4.5

Here 'M' corresponds to male and 'F' corresponds to female.

from the thenar/hypothenar of the non-dominant hand for all the datasets in this study. The experimental details are given in [44]. The total number of participants is 110 based on the experimental details in [44]. However, data for one participant is missing in Dataset 3 in the online repository. Therefore, we performed our analysis on the rest of the 109 available participants. The reported information in Table I is based on the downloaded datasets.

B. Model Formulation

As previously mentioned, the SC signal can be thought of as the summation of two different components, i.e. the tonic component and the phasic component. We consider a third component in the formulation representing the measurement noise. The SC signal can be represented combining these three components as follows:

$$y(t) = y_p(t) + y_s(t) + \nu(t),$$
 (1)

where y(t), $y_p(t)$, $y_s(t)$, and $\nu(t)$ represent the SC signal, phasic component, tonic component, and noise, respectively.

1) Phasic Component: The phasic component can be thought of as the smoothed version of the neural activity from the SNS. The smoothing is performed by the physiological system composed of a collection of sweat glands, epidermis, and other related skin components. We model the physiological system responsible for smoothing operation using the first-order kinetics of diffusion of sweat from the sweat ducts to the strata cornea and the subsequent first-order kinetics of evaporation from the strata cornea [2], [4], [6]. We combine both diffusion and evaporation kinetics to form the following second-order differential equation, and we relate it to the

neural stimuli u(t) generated by SNS:

$$\tau_r \tau_d \frac{d^2 y_p(t)}{dt^2} + (\tau_r + \tau_d) \frac{dy_p(t)}{dt} + y_p(t) = u(t),$$
 (2)

where τ_r and τ_d represent the rise and decay times for each SCR, respectively. We assume that τ_r and τ_d stay constant during the experiment, however, they can be different from person to person. Let SCR shape parameter vector τ = $[\tau_r \quad \tau_d]^{\top}$. Similar to [29]–[31], [33]–[35], we define an abstract definition of u(t) as the summation of N weighted and shifted impulse functions, i.e. $u(t) = \sum_{i=0}^{N-1} u_i \delta(t - \Delta_i)$, where u_i represents the amplitude of the neural stimulus from SNS at time Δ_i . In this study, we define $\Delta_i = iT_u$, where T_u is the sampling interval of u(t) in discrete model described in II-B.3. We define N to represent the number of samples in the discrete form of u(t), and we write it as a function of the SC signal duration T_d $(N = \frac{T_d}{T_u})$; u_i is zero if there is no neural impulse and is a positive value if there exists an impulse at time instance iT_u . Since the number of impulses in the neural stimuli is very small compared to the number of samples in the recorded SC signal, we can represent the neural stimuli as a sparse vector in discrete domain for our analysis similar to [30].

We solve the differential equation in (2) assuming the sweat duct is empty at time t=0, similar to [2], [29]–[31]. Hence, the solution to the differential equation becomes,

$$y_p(t) = y_p(0)e^{-\frac{t}{\tau_d}} + h_{\tau}(t) * u(t), \tag{3}$$

where $h_{\tau}(t)$ refers to the system impulse response representing an SCR shape and can be represented as a scaled version of the Bateman function. Here, the operator '*' represents the convolution operation. $h_{\tau}(t)$ can be written as follows,

$$h_{\tau}(t) = \begin{cases} \frac{1}{\tau_r - \tau_d} \left(e^{-\frac{t}{\tau_r}} - e^{-\frac{t}{\tau_d}} \right) & ; & \text{if } t \ge 0\\ 0 & ; & \text{otherwise} \end{cases}$$
 (4)

2) Tonic Component: We utilize a summation of several shifted and weighted cubic B-spline functions to model the tonic component as in [45] and represent it with the following convolution operation,

$$y_s(t) = \psi(t) * q(t), \tag{5}$$

where $\psi(t)$ is the cubic B-spline function and $q(t)=\sum_{j=0}^{P-1}q_j\delta(t-(j-1)\Lambda_s)$ is an alternate representation of the cubic B-spline functions coefficients denoting the scaling and

shifting operations. Here, P is the number of different shifted and scaled cubic B-spline waves used. Λ_s is the knot size of the cubic B-spline function, which is an indicator of the smoothness of the tonic component. In this study, we select $\Lambda_s=6$ seconds, the same as the maximum value of the decay time that we allow. We choose this value assuming a small increase in the tonic component during an SCR [2].

3) Discrete Model: If SC is periodically sampled with a period of T_y for M measurements, we can write the discrete observation equation as follows:

$$y_k = y_p(kT_y) + y_s(kT_y) + \nu_k,$$
 (6)

where $k \in \{1, 2, \dots, M\}$ and ν_k represents the discrete measurement errors. We model ν_k as a zero mean Gaussian random variable. As we are interested in estimating the model unknowns, we write the discrete model for y_k as follows based on (3) and (5):

$$y_k = \underbrace{a_k y_{p_0} + \mathbf{b}_k \mathbf{u}}_{\text{phasic}} + \underbrace{\mathbf{c}_k \mathbf{q}}_{\text{tonic}} + \nu_k, \tag{7}$$

where
$$a_k = e^{-\frac{kT_y}{\tau_d}}$$
, $\mathbf{b}_k = \begin{bmatrix} h_{\boldsymbol{\tau}}(kT_y) & h_{\boldsymbol{\tau}}(kT_y - T_u) & \cdots & h_{\boldsymbol{\tau}}(T_u) & \underbrace{0 \cdots 0}_{N - \frac{kT_y}{T_u}} \end{bmatrix}^{\mathsf{T}}$, $\mathbf{c}_k = \begin{bmatrix} \psi(kT_y + T_u) & \cdots & \cdots & \cdots \end{bmatrix}^{\mathsf{T}}$

 $\Lambda_s) \ \psi(kT_y) \ \psi(kT_y-\Lambda_s) \ \cdots \ \psi(kT_y-(P-1)\Lambda_s)]^{\top}$; $\mathbf{u}=[u_1 \ u_2 \ \cdots \ u_N]^{\top}$ represents a sparse vector containing all the input neural stimuli amplitudes over the entire signal duration and $\mathbf{q}=[q_1 \ q_2 \ \cdots \ q_N]^{\top}$ represents all the coefficients of the cubic B-spline basis functions and $y_{p_0}=y_p(0)$. Let $\mathbf{y}=[y_1 \ y_2 \ \cdots \ y_M]^{\top}, \ \mathbf{A}_{\tau}=[a_1 \ a_2 \ \cdots \ a_M]^{\top}, \ \mathbf{B}_{\tau}=[\mathbf{b}_1 \ \mathbf{b}_2 \ \cdots \ \mathbf{b}_M]^{\top}, \ \mathbf{C}=[\mathbf{c}_1 \ \mathbf{c}_2 \ \cdots \ \mathbf{c}_M]^{\top}, \ \mathrm{and} \ \boldsymbol{\nu}=[\nu_1 \ \nu_2 \ \cdots \ \nu_M]^{\top}. \ \mathrm{As} \ y_{p_0} \ \mathrm{is} \ \mathrm{unknown}, \ \mathrm{we} \ \mathrm{also} \ \mathrm{consider} \ \mathrm{it} \ \mathrm{as} \ \mathrm{an} \ \mathrm{unknown}, \ \mathrm{we} \ \mathrm{plan} \ \mathrm{to} \ \mathrm{estimate}. \ \mathrm{We} \ \mathrm{assume}, \ T_y=LT_u, \ \mathrm{where} \ L \ \mathrm{is} \ \mathrm{an} \ \mathrm{integer}. \ \mathrm{Please} \ \mathrm{see} \ \mathrm{supplementary} \ \mathrm{information} \ \mathrm{for} \ \mathrm{details} \ \mathrm{on} \ \psi(t) \ \mathrm{generation}. \ \mathrm{Now} \ \mathrm{the} \ \mathrm{sampled} \ \mathrm{data} \ \mathrm{vector} \ \mathbf{y} \ \mathrm{is} \ \mathrm{related} \ \mathrm{to} \ \mathrm{the} \ \mathrm{sparse} \ \mathrm{vector} \ \mathbf{u} \ \mathrm{representing} \ \mathrm{the} \ \mathrm{neural} \ \mathrm{stimuli} \ \mathrm{through} \ \mathrm{the} \ \mathrm{following} \ \mathrm{equation} \ \mathrm{equation}$

$$\mathbf{y} = \underbrace{\mathbf{A}_{\tau} y_{p_0} + \mathbf{B}_{\tau} \mathbf{u}}_{\text{phasic}} + \underbrace{\mathbf{C} \mathbf{q}}_{\text{tonic}} + \nu. \tag{8}$$

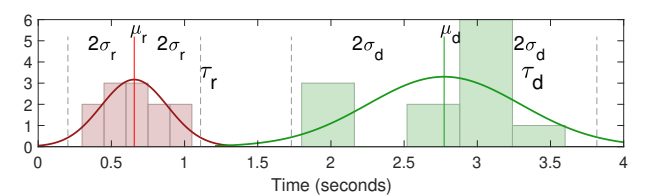


Fig. 2. Histograms of the Estimated SCR Shape Parameters in [32]: Red and green bar plots correspond to the histogram plots of the estimated rise time τ_r and decay time τ_d in [32], respectively. Red and green curve correspond to the corresponding fitted normal distribution probability distribution function. Red and green vertical line correspond to the locations of the means μ_r and μ_d of the corresponding distributions, respectively. σ_r and σ_d denote the stand deviations of the respective distributions.

4) Priors on SCR Shape Parameters: Different SCR shape parameters have been explored for deconvolution in several studies [6], [7]. Previously, prior knowledge on the SCR shapes helped the development of fixed-parameter based approaches [6], [7]. However, the use of fixed SCR shape parameters makes it very difficult to obtain accurate estimation. On the contrary, the manual selection of the SCR shape parameters can be very cumbersome and time-consuming. Recent advancements of the sparse system identification based approaches iterate between sparse neural stimuli estimation and SCR shape parameters estimation step in a coordinate descent manner [29]-[32]. In our previous study in [1], we incorporate tonic component separation along with the estimation of the SCR shape parameters. The approach showed promising results in separating the tonic component along with finding a solution for the neural stimuli and SCR shape parameters. However, this might not hold in a worst-case scenario. In some cases, the minimum might not be achieved inside the physiologically feasible set when the problem has many degrees of freedom, and it might be achieved on the boundaries. Moreover, additional flexibility of estimation SCR shape parameters in the optimization formulation may lead to over-fitting [46]. To avoid such scenarios, we include physiological priors while solving the optimization problem similar to [47]. We assume that the individual SCR shape parameters are Gaussian distributed with some mean and variance. Figure 2 shows the distribution of the estimated parameters in our previous work [32]. Later, we use this information as a prior in the optimization formulation.

C. Estimation

1) Optimization Problem Formulation: We use the same approach as in our previous work [32] for pre-processing step which is provided in the supplementary materials. After pre-processing, we obtain y with 2 Hz sampling frequency (i.e. $T_y=0.5$ seconds). We would like to recover ${\bf u}$ with 4 Hz sampling frequency (i.e. $T_u=0.25$ seconds). In order to estimate ${\bf u}$, ${\bf \theta}$, and ${\bf q}$, using discrete representation in (8), we formulate the following optimization problem while assuming the sparsity constraint on ${\bf u}$ and constraining tonic component as always less than or equal to the SC signal (i. e., ${\bf Cq} \leq {\bf y}$):

where $\boldsymbol{\tau}^{\max}$ and $\boldsymbol{\tau}^{\min}$ are the upper and lower bound of the SCR shape parameters. Here, we include the l_2 -norm penalization term with regularization parameter λ_1 to avoid over-fitting while solving for the tonic component coefficients \mathbf{q} . The above optimization formulation is a sparse recovery problem as $||\mathbf{u}||_0 \ll M < N$, where M is the number of samples in \mathbf{y} . We encourage the sparsity for \mathbf{u} with l_p -norm $(0 regularization as a relaxation to the <math>l_0$ -norm. We

re-write the optimization problem as follows:

$$\label{eq:minimize} \begin{split} \underset{\boldsymbol{\theta}, \mathbf{u}, \boldsymbol{q}}{\text{minimize}} \quad J(\boldsymbol{\theta}, \mathbf{u}, \boldsymbol{q}) &= \frac{1}{2} ||\mathbf{y} - \mathbf{A}_{\tau} y_{p_0} - \mathbf{B}_{\tau} \mathbf{u} - \mathbf{C} \mathbf{q}||_2^2 \\ &\quad + \lambda_1 ||\mathbf{q}||_2^2 + \lambda_2 ||\mathbf{u}||_p^p \\ \text{subject to} \quad \boldsymbol{\tau}^{\min} &\preccurlyeq \boldsymbol{\tau} \preccurlyeq \boldsymbol{\tau}^{\max}, 0 \leq y_{p_0} \leq y_1, \\ &\quad \mathbf{u} \succcurlyeq 0, \; \mathbf{C} \mathbf{q} \preccurlyeq \mathbf{y}, \end{split}$$

where λ_2 is a regularization parameter which determines the sparsity level for **u**. We can solve the inverse problem of finding a non-negative **u** in (9) with a specific sparsity level using the iterative least squares (IRLS) approach Focal Underdetermined System Solver (FOCUSS+) algorithm [48].

Finally, inspired by the work in [47], we also consider the priors on SCR shape parameters based on the estimations in [32]. We assume that among different individual the rise times τ_r and decay times τ_d are Gaussian distributed with means μ_r and μ_d with corresponding standard deviations σ_r and σ_d , respectively. The optimization formulation with the priors on the SCR shape parameters becomes as follows:

subject to
$$\boldsymbol{\tau}^{\min} \preccurlyeq \boldsymbol{\tau} \preccurlyeq \boldsymbol{\tau}^{\max}, 0 \leq y_{p_0} \leq y_1, \mathbf{u} \geq 0, \mathbf{Cq} \preccurlyeq \mathbf{y},$$

where λ_3 and λ_4 are the regularization parameters. In this work, we use $\lambda_3 = \lambda_4 = 1 \times 10^{-1}$. We select $\mu_r = 0.650571$, $\mu_d = 2.77325$, $\sigma_r = 0.212443$ and $\sigma_d = 0.521739$ based on the results in [32].

2) Generalized Cross-Validation for λ_1 and λ_2 : We used the following GCV function to have a valid definition for tall matrix C for estimating λ_1 [49],

minimize
$$G_1(\lambda_1) = \frac{M||(\mathbf{I} - \mathbf{H}_{\lambda_1})\hat{\mathbf{y}}_s||_2^2}{(\operatorname{Trace}(\mathbf{I} - \mathbf{H}_{\lambda_1}))^2}$$
 (11) subject to $\mathbf{0} \le \lambda_1 \le 1 \times 10^{-4}$,

where $\hat{\boldsymbol{y}}_s = (\mathbf{y} - \mathbf{A}_{\tau} y_{p_0} - \mathbf{B}_{\tau} \mathbf{u})$ and \mathbf{H}_{λ_1} is the influence matrix. For this case, $\mathbf{H}_{\lambda_1} = \mathbf{C}(\mathbf{C}^{\top}\mathbf{C} + \lambda_1 \mathbf{I})\mathbf{C}^{\top}$.

FOCUSS+ allows us to obtain a solution for \mathbf{u} such that the number of non-zero elements is predefined. We use FOCUSS+ for the initialization step. Once a reasonable initialization has been obtained, in each iteration of the IRLS algorithm, we use GCV for estimating an appropriate regularization parameter λ_2 similar to [29], [30], [34], [35]. This combination of GCV and FOCUSS+ algorithm is known as GCV-FOCUSS+ [50]. Zdunek *et al.* [50] used the following optimization formulation with singular value decomposition (SVD) for GCV:

minimize
$$G_2(\lambda_2) = \frac{\left[M \sum_{i=1}^{M} \gamma_i^2 \left(\frac{\lambda_2}{\sigma_i^2 + \lambda_2}\right)^2\right]}{\left[\sum_{i=1}^{M} \left(\frac{\lambda_2}{\sigma_i^2 + \lambda_2}\right)^2\right]}$$
 (12)

subject to
$$0 \le \lambda_2 \le 1 \times 10^{-4}$$

where
$$\boldsymbol{\gamma} = \mathbf{R}^{\top} \mathbf{y}_{\tau} = \begin{bmatrix} \gamma_1 & \gamma_2 & \cdots & \gamma_M \end{bmatrix}^{\top}$$
 with $\mathbf{y}_{\tau} = \mathbf{y} - \mathbf{A}_{\tau} y_{p_0} - \mathbf{C} \mathbf{q}$, and $\mathbf{B}_{\tau} \mathbf{P}_{\mathbf{u}}^{\frac{1}{2}} = \mathbf{R} \boldsymbol{\Sigma} \mathbf{Q}^{\top}$ with $\mathbf{P}_{\mathbf{u}} = \operatorname{diag}(|\mathbf{u}_i|^{2-p})$

and $\Sigma = \text{diag}\{\sigma_i\}$; **R** and **Q** are unitary matrices and σ_i 's are the singular values of $\mathbf{B}_{\tau}\mathbf{P}_{\mathbf{u}}^{\frac{1}{2}}$. The details of GCV-FOCUSS+ is given in supplementary information.

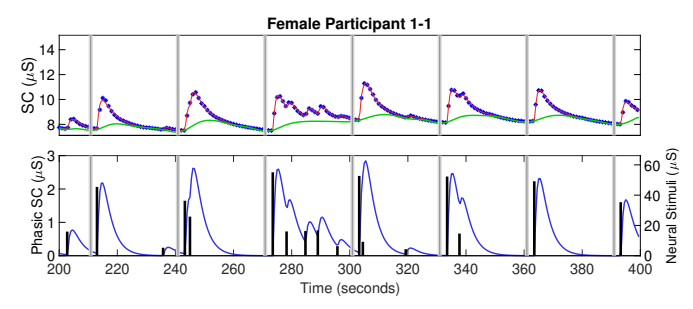
We use a coordinate descent algorithm similar to our previous work in [1] to solve the optimization problem in (10). The detailed algorithm is provided in the supplementary materials. We run the algorithm for several random initializations of θ and take the result that minimizes the least square error between the observed and reconstructed signal.

III. RESULTS

We have applied our approach and decompose the SC measurements recorded from 109 participants from five datasets provided in Table I and separate the tonic components $y_s(t)$ and phasic components $y_p(t)$. During each decomposition, we have recovered the underlying neural stimuli u(t), rise time (τ_r) , decay time (τ_d) , and the initial condition of the phasic component y_{p_0} . We have considered the signal segment from 200 seconds to 400 seconds for our analysis for Dataset 1, 2, 4, and 5. For Dataset 3, we have considered the signal segment from 100 seconds to 300 seconds for our analysis as the experimental duration for some of the participants is shorter than 400 seconds. Figure 3 shows example results for one female participant and one male participant. Figure 3 shows that we are successfully able to detect the SNS activation after each auditory stimulation. The rest of the results from experimental data are provided in supplementary materials. The estimated rise time (τ_r) , decay time, number of pulses $(||\mathbf{u}||_0)$, multiple correlation coefficient (R^2) , regularization parameters (λ_1 and λ_2), deconvolution run-times are provided in the supplementary material for all 26 participants from Dataset 1.

Figure 5 shows the histogram of the estimated SCR shape parameters from 109 participants. Means of the histograms are estimated to be $\mu_r=0.7274$ and $\mu_d=2.8629$ seconds for rise times and decay times, respectively. Corresponding standard deviations are $\sigma_r=0.1146$ and $\sigma_d=0.1491$ seconds, respectively. The R^2 values are greater than 0.95 for all participants. The high values of R^2 SC data suggest that our proposed algorithm can successfully decompose the SC recording in its constituent components and separate the tonic and phasic components. The corresponding quantile-quantile plots for the model residuals are also given in the supplementary materials. The quantile-quantile plots approximately follow a straight line denoting the Gaussian structure in the residuals. Slight deviations from the straight line also suggest that there is a scope of improvement in the system model.

To perform an efficacy analysis of how our algorithm performs in distinguishing between event-related and non-event-related SCRs in Dataset 1, we have derived receiver operating characteristics (ROC) curves [51]. We label all the SCRs that have been detected within 5 seconds after auditory stimuli as the event-related SCRs (positive class). The rest of the detected SCRs are labeled as the non-event-related SCRs (negative class). We consider the amplitudes of the SCRs as the classification scores within the subjects for obtaining the ROC curves [51], [52]. The results show that the ROC curves



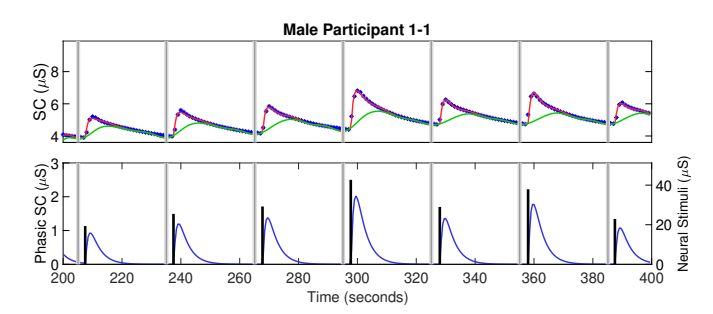
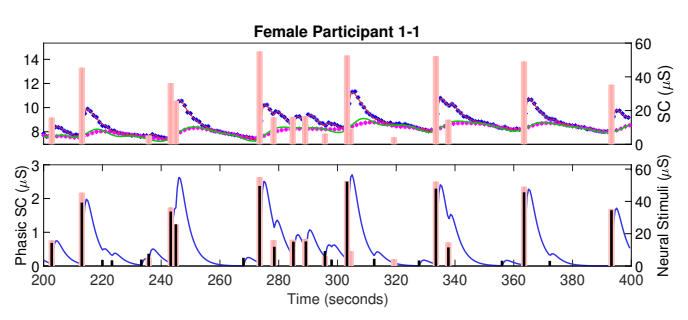


Fig. 3. Estimated Decomposition of the Experimental SC Signals for One Female Participant and One Male Participant: In each of the panels, i) the top sub-panel shows the experimental SC signal (blue stars), the reconstructed SC signal (red curve), the estimated tonic component (green curve), and the timings of the auditory stimulations (gray vertical lines); ii) the bottom sub-panel shows the estimated phasic component (blue curve), estimated neural stimuli timings and amplitudes (black vertical lines) due to SNS activation and the timings of the auditory stimuli (gray vertical lines). The number before the hyphen in the participant ID represents the dataset ID based on Table I



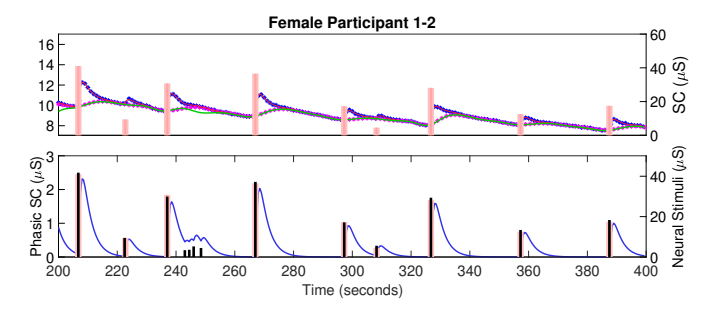


Fig. 4. Estimated Decomposition of the Simulated SC Signals with 25 dB SNR for One Female Participant and One Male Participant: In each of the panels, i) the top sub-panel shows the ground truth for SC signal (blue stars), the reconstructed SC signal (red curve), the ground truth for tonic component (red stars), the estimated tonic component (red curve), and ground truth for the neural stimuli (pink vertical lines); ii) the bottom sub-panel shows the estimated phasic component (blue curve), estimated neural stimuli timings and amplitudes (black vertical lines) due to SNS activation and the ground truth for the neural stimuli (gray vertical lines). The number before the hyphen in the participant ID represents the dataset ID based on Table I

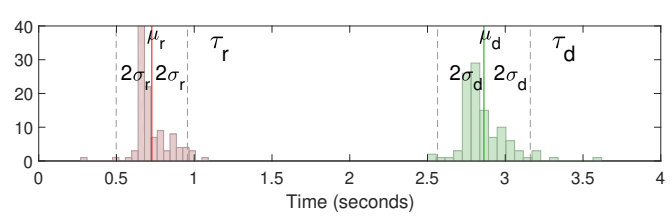


Fig. 5. Histograms of Estimated SCR Shape Parameters using Our Approach: Red and green bar plots correspond to the histogram plots of the estimated rise time τ_r and decay time τ_d , respectively. Red and green vertical line correspond to the locations of the means μ_r and μ_d of the corresponding histograms, respectively. σ_r and σ_d denote the corresponding standard deviations, respectively.

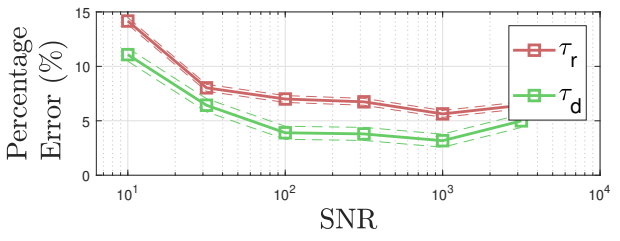


Fig. 6. Estimation Accuracy of SCR Shape Parameters in Different Noise Levels: Red and green solid lines denotes the mean percentage error for rise times and decay times from simulated data with different noise levels. The dashed lines corresponds to the 95% confidence interval. The data is simulated using the obtained results from the experimental data in Dataset 1. As noise is added to the phasic component prior to addition of tonic component, the SNR is given with respect to the phasic component.

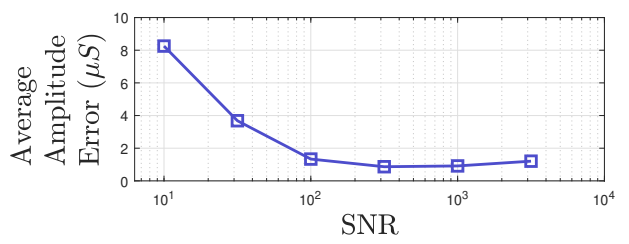


Fig. 7. Average Amplitude Error of Estimated Neural Stimuli in Different Noise Levels: The blue solid line denotes the average amplitude error of the neural stimuli from estimated data with different noise levels. We have defined the average amplitude error as $||\tilde{\mathbf{u}}||_1 - ||\mathbf{u}||_1/||\mathbf{u}||_0$, where $\tilde{\mathbf{u}}$ and \mathbf{u} represent the estimated and the ground truth neural stimuli, respectively. The data is simulated using the obtained results from the all experimental data in Dataset 1. As noise is added to the phasic component prior to addition of tonic component, the SNR is given with respect to the phasic component.

have the area under the curve (AUC) ranging from 0.5611 to 1 with a median of 0.8636 and a mean of 0.9130. Moreover, we normalized the estimated **u** for each participant and combine them to obtain an overall ROC curve. The corresponding overall AUC is 0.864 for Dataset 1. All the ROC curves are provided in supplementary materials.

We simulate data with noise to investigate the efficacy of our approach. We use the results obtained from Dataset 1 to simulate data for 26 participants. In this case, we have ground truths to compare with the estimated unknowns. Our deconvolution approach successfully estimates neural stimuli along with the SCR shape parameters, i.e. the physiological

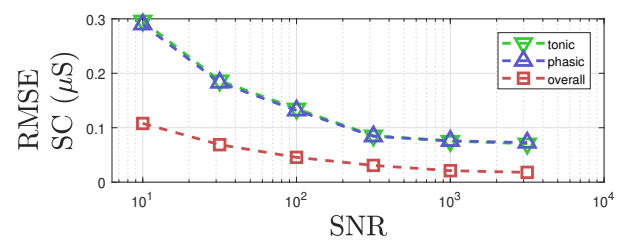


Fig. 8. Root Mean Square Error (RMSE) of the Reconstructio for SC signal and Corresponding Components with Respect to th Ground Truth: Green, blue and red dashed lines denote the RMSE fr the reconstructed tonic component, phasic component and overall S data in different noise levels. The data is simulated using the obtaine results from the all experimental data in Dataset 1. As noise is added the phasic component prior to addition of tonic component, the SNR given with respect to the phasic component.

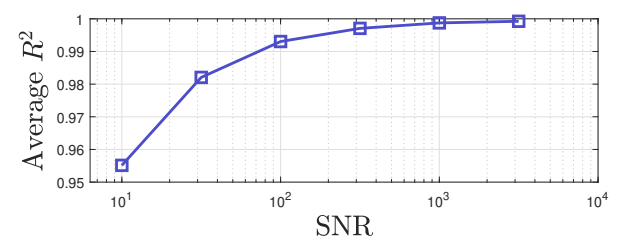
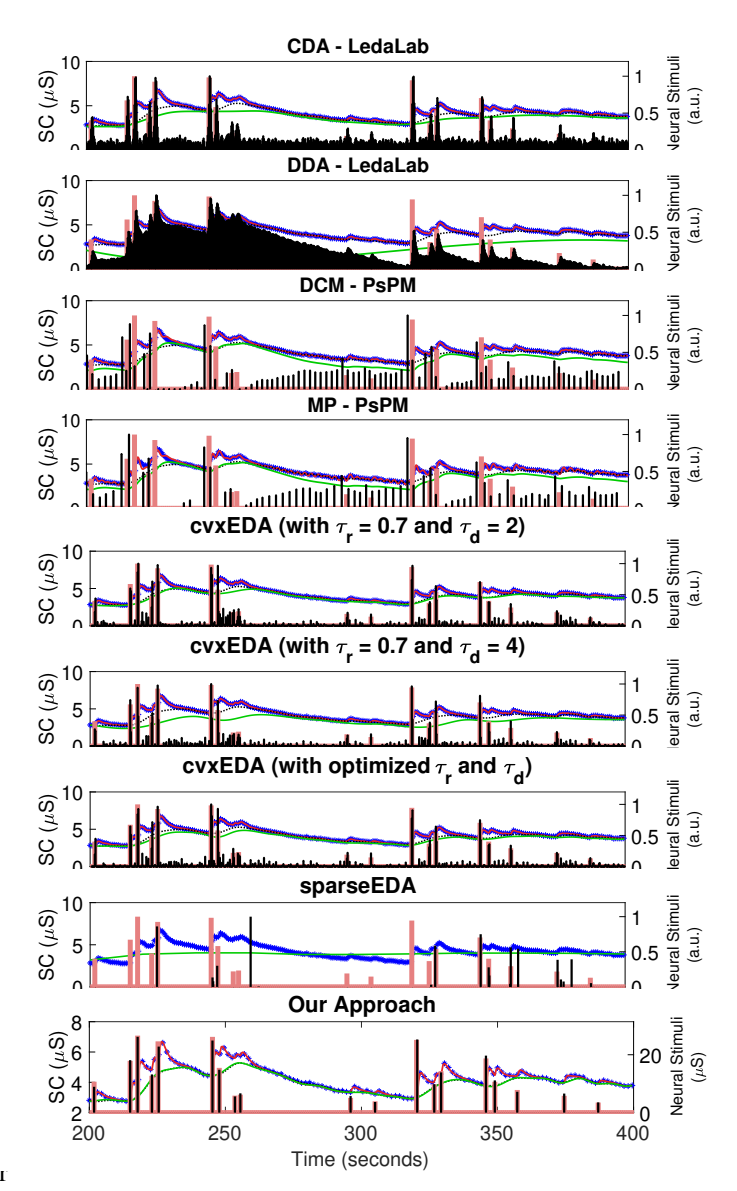


Fig. 9. R^2 SC signal reconstruction: Blue solid line denotes the mean R^2 values for the reconstructed SC data with different noise levels. The data is simulated using the obtained results from the all experiments data in Dataset 1. As noise is added to the phasic component prior to addition of tonic component, the SNR is given with respect to the phasic component.

system parameters. Figure 4 shows example deconvolution from simulated data for one female and one male participant with 25 dB SNR with respect to phasic component. The minimum R^2 for the simulated data with 25 dB noise leve is 0.9872. Figures, estimated system parameters $(\hat{\tau}_r$ and $\hat{\tau}_d)$ estimated number of pulses $(||\hat{\mathbf{u}}||_0)$, estimation errors, and the multiple correlation coefficients (R^2) for the results for all the simulated data with 25 dB SNR are provided in the supplementary materials.

We also simulate data with different noise levels to see how our approach performs in terms of estimating the unknowns and reconstructed signal. We have used the results obtained from the experimental recordings for all 26 participants to generate 26 signals for each level of noise. We have performed deconvolution to estimate the SCR shape parameters. Afterwards, we have calculated the percentage error for each of the participants. Figure 6 and 7 show how the average estimation error increase as the noise level is increased. Similarly, Figure 8 shows how the reconstruction error decreases and Figure 9 shows how the R^2 value decreases with the increase in the noise level.

To compare our method with the other existing approaches, we have used synthetic simulated data. We have used the neural stimuli, the SCR shape parameters, and the cubic-spline coefficients obtained from the deconvolution of the experimental recordings of male subject six to simulate the data. We have added Gaussian random noise with 25 dB SNR with respect to the phasic component. We have simulated the data with two different sampling frequencies. We simulated



Performance Comparison of Proposed Approach with Fig. 10. Existing Approaches for Simulated Data: Each panel shows the decomposition performance based on simulated SC signal with 25 dB noise. The panels from top to bottom show the results obtained using CDA - LedaLab [5], DDA - LedaLab [6], DCM - PsPM [25], MP - PsPM [26], cvxEDA with three different configurations [7], sparsEDA [28], and our proposed approach, respectively. In each panel, blue stars represent the simulated data, pink vertical lines represent the ground truth neural stimuli, black vertical lines represent the recovered neural stimuli, the green curve represents the tonic component, the black dotted curve represents the ground truth for the tonic component, and the red curve represents the reconstructed signal. The estimated neural stimuli for all the panels except for the last one are normalized from zero to one to avoid any amplitude scaling originating from different methods and to have a fair comparison.

data with 2 Hz sampling frequency for performing deconvolution with our approach. For other methods, we chose a 4 Hz sampling frequency. We specifically do this to show that even with lower sampling frequency, our algorithm performs reasonably well and able to obtain ${\bf u}$ with 4Hz resolution while performing in a compressed sensing regime (M < N). Figure 10 shows the decomposition of tonic, phasic component, and recovered neural stimuli using CDA - LedaLab [5], DDA -

LedaLab [6], DCM - PsPM [25], MP - PsPM [26], cvxEDA with three different configurations [7], sparsEDA [28], and our proposed approach. We have used default settings for the parameters for all the approaches except for cvxEDA and sparsEDA. For cvxEDA, we have used the knot size for cubic B-spline functions to be the same as our approach for a fair comparison. Further, we have considered three different configurations for τ_r and τ_d including optimized parameters from our approach for cvxEDA.We perform the comparison with different physiological parameters only with cvxEDA because it considers similar system modeling and optimization formulation as ours. Therefore, this comparison will be fair if carried out against cvxEDA. The results show there are differences in the solution for different selected parameters. In the case of sparsEDA, we have selected the minimum separation between two neural impulses and the threshold for the neural impulse amplitudes to be zero to have the most less sparse solution. DCM - PsPM and MP - PsPM perform linear band-pass filtering for removing the tonic component followed by a DC shift to avoid all the negative value in the phasic. We have performed the adjustments to the obtained results accordingly so that the visual comparison is fair. Qualitatively, the results show that our algorithm is performing well in terms of capturing the neural stimuli related to the SCRs and discarding small spikes which are comparable to noise spikes. DCM - PsPM and MP - PsPM detects large pulses where there are no pulses mainly because the signal is distorted in the preprocessing step. As observed in Figure 10, other approaches except sparsEDA are providing less sparse solutions compared to the ground truth. Some of the pulses detected by these algorithms are capturing noise. In this case, our proposed approach is performing well in balancing between the sparsity level and discarding noise. On the other hand, sparsEDA is providing an overly sparse solution leading to missing some of the obvious neural impulses captured by all the other algorithms.

In order to perform further comparison between the deconvolution results from different algorithms, we have added noise noise to the raw experimental data. The noise level is selected in a way that the signal SNR is 25 dB for corresponding phasic component estimated during deconvolution. We performed deconvolution on six participants as example. The results are shown in supplementary materials.

IV. DISCUSSIONS

Decomposition of SC signals into its constituents along with the estimation of the neural stimuli, the rise and decay times of the SCRs is challenging. The challenges includes identification of the sparsity level for the neural stimuli as well as the smoothness of the tonic component. An inaccurate estimation for the smoothness of the tonic component can make the estimation of rise times and decay times inaccurate. As least square formulation has many degrees of freedom, optimization without appropriate physiological constraints may lead to a problem that is not identifiable. The problem becomes much more challenging in the case of under-determined systems, i.e. when the M < N. Presence of the smallest amount of noise

can lead the system response to a physiologically infeasible solution. We incorporate necessary physiologically plausible constraints to make the optimization problem tractable. Firstly, we consider the sparsity constraint on the neural stimuli. In our previous works in [1], [30]–[32], we constrained the SCR shape parameters within physiologically feasible bounds $(\tau^{\min} = \begin{bmatrix} 0.10 & 1.5 \end{bmatrix}^{\top}$ and $\tau^{\max} = \begin{bmatrix} 1.5 & 6 \end{bmatrix}^{\top}$). In addition to that, we impose Gaussian priors on τ_r and τ_d . Further, we have chosen the regularization parameters λ_3 and λ_4 such that the solution for τ_r and τ_d do not converge to the boundary. To achieve that, we have first started with a very small value of λ_3 and λ_4 such 1×10^{-5} and ran deconvolution on random selected twelve participants from Dataset 1. However, for some of the participants, the solution for τ_r and τ_d converges to the boundary. Therefore, we gradually increase λ_3 and λ_4 by a factor of 10 until all the stagnation to boundary is avoided. Afterward, we fix the λ_3 and λ_4 for the rest of the 97 participants from all the five datasets. Figure 5 show that none of the estimated parameters are near the boundary constraint. We also impose constraints on the smoothness of the cubic B-spline basis function by including l_2 -norm penalization. Finally, we incorporate the GCV technique [49] to have appropriate estimates of λ_1 and λ_2 to achieve a balance between capturing the data and residual error.

As we previously mentioned in [30], although the optimization problem in (10) is convex in terms of \mathbf{u} and \mathbf{q} [1], [7], it is non-convex for τ . During the iterations of coordinate descent, the solution may stagnate at local minima. The stagnation of solution at a local minima leads to an inaccurate separation of tonic and phasic components, some part of the tonic component might be captured in the phasic component. Therefore, we initialize the optimization problem with several random initializations for SCR shape parameters au. Among all the deconvolution results using these random initializations, we choose the one that minimizes the least square error. The larger number of random initializations means a greater probability of obtaining global minima, i.e. there is a trade-off between the probability of obtaining the optimal solution and the number of random initializations. In this study, we have considered eight random initializations for the system parameters and we ran in the eight CPU cores in parallel. This way we reduce the probability of convergence to a local minimum. Although it is still possible to converge a sub-optimal solution, we have empirically demonstrated on experimental data collected from 109 participants shown that our algorithm is performing well in terms of modeling the SCR shapes and reducing the number of the unwanted pulse due to incorrect shape parameters. Moreover, based on the simulated study, Figure 6 shows that our approach can reliably estimate the SCR shape parameters with only eight initializations for moderate noise levels.

In this study, we obtain **u** with a higher resolution than the recorded signal. For instance, in our study, the sparse vector **u** has a length of 800 with 4 Hz sampling frequency while the sampled signal has 400 samples with 2 Hz sampling frequency. We are specifically interested in the accurate timing and amplitude of the SNS activation rather than the phasic component. In contrast, we are more interested in the tonic

component itself rather than its cubic B-spline coefficients as the exact cause and appropriate system theoretic modeling of tonic component is unknown. Further, as the body tries to regulate its skin moisture, i.e. the tonic component depending on the cooling demand in the body. Tonic component itself is an indication of the factor related to the thermoregulation rather than its coefficients. Therefore, we use much less number of coefficients in vector ${\bf q}$ in order to model the tonic components compared to ${\bf u}$. In this study, we have used 39 coefficients to model 200 seconds of SC signal.

Noise can corrupt SC signal, and sometimes small noise spikes can be comparable to the small insignificant SCRs. To avoid such cases, we used an internal threshold in each iteration of GCV-FOCUSS+ part while estimating u. If an estimated non-zero element in **u** is smaller than the threshold, that particular value is set to be zero. In this study, we used 3 as the threshold. This threshold works well for almost all the experimental and simulated data. However, our algorithm has detected some small noise spikes as SCRs in simulated data for a few participants. The reason of detecting more spike for these signals is that there are more noise added to these signals compared to the other signals. Although we mentioned we have added noise so that SNR is 25 dB, the SNR value of the simulated data is with respect to phasic component. For these particular simulated signals, the phasic components have more energy compared to the other simulated signals. Because of this corresponding noise power is also higher. Some noise peak amplitudes are comparable to noise and in few places they have been detected as SCRs. Furthermore, the estimation of tonic component is also slightly inaccurate in places where there is a noise spike that has been detected as an SCR. However, this only happens for a few badly condition cases where noise level is comparable to SCRs.

From our results, we can see the \mathbb{R}^2 values are close to 1, denoting that model fits are very good in case of reasonable noise level. Quantile-quantile plots in the supplementary material also follow approximately a straight line. However, there are still slight deviations from the straight line in the quantile-quantile plots for a few experimental data although for simulated data there no such case. This indicates there is a scope of improvement in the system modeling. Specially modeling tonic component with arbitrary cubic B-spline function might not be the most effective way to model the tonic component. Therefore, there is a need for development of tonic component with systematic way based on physiology.

As three unknowns (i.e. \mathbf{u} , \mathbf{q} , and $\boldsymbol{\theta}$) have been solved in a coordinate descent manner along with the GCV technique to minimize the optimization problem in (10) with appropriate physiologically plausible solution, it takes more time to complete the deconvolution compared to some of the previous methods. The time elapsed for the deconvolution with our approach for Dataset 1 is provided in the supplementary materials. The deconvolution time required for LedaLab (CDA), LedaLab(DDA), PsPM (DCM), PsPM (MP), cvxEDA, sparsEDA and our approach for the deconvolution comparison shown in Figure 10 is respectively 1.45 seconds, 8.05 seconds, 153.23 seconds, 0.3162 seconds, 0.211 seconds, 0.1563 seconds, and 89.95 seconds. The other approaches do

not concurrently optimize the problem for the SCR shape parameters, the sparsity neural stimuli, and the smoothness level of the tonic component. Although our approach takes more time to deconvolve, our approach outperforms previous approaches in terms of balancing between discarding the noise and capturing significant SCRs.

Perhaps, the most appropriate way of evaluating a method would be to use a dataset that contains the recording from the nerve endings to the sweat glands and the corresponding SC recording similar to the study in [53]. However, we could not perform such a comparison because of the unavailability of such datasets. Bach et al. [54] have suggested evaluating metrics by an algorithm's ability to separating the experimental event vs the non-events or the ability to separate a high-arousal condition. We have performed a similar analysis to show our algorithm's ability to be able to distinguish between separating the experimental event-related vs the non-event-related SCRs obtained corresponding ROC curves. Nevertheless, our algorithm is designed to capture the SCRs for emotional events as well as the spontaneous SCRs which might not be related to an emotional event but originating from the natural physiological control of the body. For example, visually it can be seen that for some participants, there are a lot more spontaneous pulses than the number of auditory stimuli, for some other participants the numbers of SCRs are a lot less than the numbers of provided stimuli. Therefore, there is a limitation in such an evaluation. Distinguishing between event-related and non-event-related SCRs will also heavily depend on how a detection scheme is devised for a specific algorithm and the scheme can be different for different algorithms to obtain the best performance. For example, some algorithms use some sort of thresholding as post-processing before performing the classification [25]. On the other hand, our evaluation does not involve any post-processing. Therefore, we did not perform any comparison based on such evaluation with other algorithms to avoid any unfair comparisons. The objective of the current study is not to show its ability to separate the event-related response but to perform a plausibility assessment with a large dataset of 109 participants and show its ability to capture any phasic response regardless of its reason for the occurrence. We have further demonstrated the performance evaluation of our approach in terms of estimating neural stimuli and the physiological system parameters in simulated data at different noise levels. Further, we qualitatively demonstrate how results from our approach compare with other approaches. The qualitative comparison shows that results are correlated, and our approach is performing better in terms of balancing between noise reduction and capturing the underlying physiological phenomenon. Apart from the visual demonstration for comparisons with different previous algorithms, we have also included a list of estimated R^2 values and the estimated numbers of neural impulses from the noisy experimental data in the supplementary information. The results show that almost the same R^2 is obtained by detecting a greater number of pulses which could be an indication of potential over-fitting for the other algorithms except for sparsEDA, where our algorithm has estimated fewer numbers of impulses but had the same level of model fit. However, the lack of comparative metrics

between different algorithms can be considered as a limitation of the study.

V. CONCLUSION

In this study, we proposed an approach to decompose SC recordings into its constituents to accurately identify the SNS generated neural stimuli to sweat glands and the physiological system parameters. We propose a GCV and coordinate descent-based deconvolution algorithm for simultaneously estimating the tonic component, neural stimuli and the physiological system parameters by automatically balancing the smoothness of the tonic component, the sparsity of neural stimuli, and the residual error. Analyzing experimental and simulated data we showed that our approach successfully uncovers the neural stimuli due to the known auditory stimulation times. We have performed comparisons with six widely used previous approaches and have qualitatively shown that our approach outperforms previous approaches in terms of balancing between the discarding noise spikes and capturing the significant neural impulses.

In the future, we plan to exploit the state-space formulation of SC and implement a Bayesian inference framework to reduce the time complexity. The obtained SNS activities can be used to track the cognitive arousal state [3], [9], [55]. For further accurate estimation of emotional arousal, we intend to utilize the inferred SNS activity from SC recording with our approach and to combine with other physiological signals similar to [17], [56]–[61]. Finally, we plan to design appropriate control measures in order to regulate the arousal level inferred using the deciphered SNS activity, similar to the strategies in [62]–[65].

REFERENCES

- [1] M. R. Amin and R. T. Faghih, "Tonic and phasic decomposition of skin conductance data: A generalized-cross-validation-based block coordinate descent approach," in 2019 41st Annual International Conference of the IEEE Engineering in Medicine and Biology Society (EMBC). IEEE, 2019, pp. 745–749.
- [2] W. Boucsein, Electrodermal activity. Springer Science & Business Media, 2012.
- [3] D. S. Wickramasuriya, C. Qi, and R. T. Faghih, "A state-space approach for detecting stress from electrodermal activity." in *Annual International Conference of the IEEE Engineering in Medicine and Biology Society. IEEE Engineering in Medicine and Biology Society. Annual Conference*, vol. 2018, 2018, pp. 3562–3567.
- [4] D. M. Alexander, C. Trengove, P. Johnston, T. Cooper, J. August, and E. Gordon, "Separating individual skin conductance responses in a short interstimulus-interval paradigm," *Journal of neuroscience methods*, vol. 146, no. 1, pp. 116–123, 2005.
- [5] M. Benedek and C. Kaernbach, "A continuous measure of phasic electrodermal activity," *Journal of neuroscience methods*, vol. 190, no. 1, pp. 80–91, 2010.
- [6] M. Benedek and C. Kaernbach, "Decomposition of skin conductance data by means of nonnegative deconvolution," *Psychophysiology*, vol. 47, no. 4, pp. 647–658, 2010.
- [7] A. Greco, G. Valenza, A. Lanata, E. P. Scilingo, and L. Citi, "cvxeda: A convex optimization approach to electrodermal activity processing," *IEEE Transactions on Biomedical Engineering*, vol. 63, no. 4, pp. 797–804, 2016.
- [8] J. J. Braithwaite, D. G. Watson, R. Jones, and M. Rowe, "A guide for analysing electrodermal activity (eda) & skin conductance responses (scrs) for psychological experiments," *Psychophysiology*, vol. 49, no. 1, pp. 1017–1034, 2013.
- [9] D. S. Wickramasuriya and R. T. Faghih, "A bayesian filtering approach for tracking arousal from binary and continuous skin conductance features," *IEEE Transactions on Biomedical Engineering*, 2019.

[10] S. Jain, U. Oswal, K. S. Xu, B. Eriksson, and J. Haupt, "A compressed sensing based decomposition of electrodermal activity signals," *IEEE Transactions on Biomedical Engineering*, vol. 64, no. 9, pp. 2142–2151, 2017.

- [11] N. Howell, L. Devendorf, R. K. Tian, T. Vega Galvez, N.-W. Gong, I. Poupyrev, E. Paulos, and K. Ryokai, "Biosignals as social cues: Ambiguity and emotional interpretation in social displays of skin conductance," in *Proceedings of the 2016 ACM Conference on Designing Interactive Systems*, 2016, pp. 865–870.
- [12] E. R. Walker, R. E. McGee, and B. G. Druss, "Mortality in mental disorders and global disease burden implications: a systematic review and meta-analysis," *JAMA psychiatry*, vol. 72, no. 4, pp. 334–341, 2015.
- [13] L. San Too, M. J. Spittal, L. Bugeja, L. Reifels, P. Butterworth, and J. Pirkis, "The association between mental disorders and suicide: A systematic review and meta-analysis of record linkage studies," *Journal* of affective disorders, 2019.
- [14] S. L. Murphy, J. Xu, K. D. Kochanek, and E. Arias, "Mortality in the united states, 2017," 2018.
- [15] D. S. Shepard, D. Gurewich, A. K. Lwin, G. A. Reed Jr, and M. M. Silverman, "Suicide and suicidal attempts in the united states: costs and policy implications," *Suicide and Life-Threatening Behavior*, vol. 46, no. 3, pp. 352–362, 2016.
- [16] J. J. Gross and H. Jazaieri, "Emotion, emotion regulation, and psychopathology: An affective science perspective," *Clinical Psychological Science*, vol. 2, no. 4, pp. 387–401, 2014.
- [17] S. Parshi, M. R. Amin, H. F. Azgomi, and R. T. Faghih, "Mental workload classification via hierarchical latent dictionary learning: A functional near infrared spectroscopy study," in *IEEE-EMBS Iternational* Conference on Biomedical and Health Informatics, May 2019.
- [18] Z. Yin, M. Zhao, Y. Wang, J. Yang, and J. Zhang, "Recognition of emotions using multimodal physiological signals and an ensemble deep learning model," *Computer methods and programs in biomedicine*, vol. 140, pp. 93–110, 2017.
- [19] B. I. Freedman, D. W. Bowden, S. C. Smith, J. Xu, and J. Divers, "Relationships between electrochemical skin conductance and kidney disease in type 2 diabetes," *Journal of Diabetes and its Complications*, vol. 28, no. 1, pp. 56–60, 2014.
- [20] B. I. Freedman, S. C. Smith, B. M. Bagwell, J. Xu, D. W. Bowden, and J. Divers, "Electrochemical skin conductance in diabetic kidney disease," *American journal of nephrology*, vol. 41, no. 6, pp. 438–447, 2015.
- [21] T. He, C. Wang, A. Zuo, P. Liu, R. Zhao, W. Li, L. Chen, and X. Hou, "Electrochemical skin conductance may be used to screen for diabetic cardiac autonomic neuropathy in a chinese population with diabetes," *Journal of diabetes research*, vol. 2017, 2017.
- [22] B. C. Callaghan, H. T. Cheng, C. L. Stables, A. L. Smith, and E. L. Feldman, "Diabetic neuropathy: clinical manifestations and current treatments," *The lancet NEUROLOGY*, vol. 11, no. 6, pp. 521–534, 2012.
- [23] N. Gerrett, K. Griggs, B. Redortier, T. Voelcker, N. Kondo, and G. Havenith, "Sweat from gland to skin surface: production, transport, and skin absorption," *Journal of Applied Physiology*, vol. 125, no. 2, pp. 459–469, 2018.
- [24] H. F. Posada-Quintero and K. H. Chon, "Innovations in electrodermal activity data collection and signal processing: A systematic review," *Sensors*, vol. 20, no. 2, p. 479, 2020.
- [25] D. R. Bach, J. Daunizeau, K. J. Friston, and R. J. Dolan, "Dynamic causal modelling of anticipatory skin conductance responses," *Biological* psychology, vol. 85, no. 1, pp. 163–170, 2010.
- [26] D. R. Bach and M. Staib, "A matching pursuit algorithm for inferring tonic sympathetic arousal from spontaneous skin conductance fluctuations," *Psychophysiology*, vol. 52, no. 8, pp. 1106–1112, 2015.
- [27] D. R. Bach, "A head-to-head comparison of scralyze and ledalab, two model-based methods for skin conductance analysis," *Biological psychology*, vol. 103, pp. 63–68, 2014.
- [28] F. Hernando-Gallego, D. Luengo, and A. Artés-Rodríguez, "Feature extraction of galvanic skin responses by non-negative sparse deconvolution," *IEEE Journal of Biomedical and Health Informatics*, 2017.
- [29] R. T. Faghih, P. A. Stokes, M.-F. Marin, R. G. Zsido, S. Zorowitz, B. L. Rosenbaum, H. Song, M. R. Milad, D. D. Dougherty, and E. N. Eskandar, "Characterization of fear conditioning and fear extinction by analysis of electrodermal activity," in *Engineering in Medicine and Biology Society (EMBC)*, 2015 37th Annual International Conference of the IEEE, 2015, pp. 7814–7818.
- [30] M. R. Amin and R. T. Faghih, "Sparse deconvolution of electrodermal activity via continuous-time system identification," *IEEE Transactions* on Biomedical Engineering, 2019.

[31] M. R. Amin and R. T. Faghih, "Inferring autonomic nervous system stimulation from hand and foot skin conductance measurements," in 52th Asilomar Conference on Signals, Systems and Computers, 2018.

- [32] M. R. Amin and R. T. Faghih, "Robust inference of autonomic nervous system activation using skin conductance measurements: A multi-channel sparse system identification approach," *IEEE Access*, vol. 7, pp. 173 419–173 437, 2019.
- [33] R. T. Faghih, "System identification of cortisol secretion: Characterizing pulsatile dynamics," Ph.D. dissertation, Massachusetts Institute of Technology, 2014.
- [34] R. T. Faghih, M. A. Dahleh, G. K. Adler, E. B. Klerman, and E. N. Brown, "Deconvolution of serum cortisol levels by using compressed sensing," *PLoS ONE*, vol. 9, no. 1, p. e85204, 2014.
- [35] R. T. Faghih, M. A. Dahleh, G. K. Adler, E. B. Klerman, and E. N. Brown, "Quantifying pituitary-adrenal dynamics and deconvolution of concurrent cortisol and adrenocorticotropic hormone data by compressed sensing," *IEEE Transactions on Biomedical Engineering*, vol. 62, no. 10, pp. 2379–2388, 2015.
- [36] R. T. Faghih, "From physiological signals to pulsatile dynamics: a sparse system identification approach," in *Dynamic Neuroscience*. Springer, 2018, pp. 239–265.
- [37] D. D. Pednekar, M. R. Amin, H. F. Azgomi, K. Aschbacher, L. J. Crofford, and R. T. Faghih, "Characterization of cortisol dysregulation in fibromyalgia and chronic fatigue syndromes: A state-space approach," *IEEE Transactions on Biomedical Engineering*, 2020.
- [38] D. D. Pednekar, M. R. Amin, H. F. Azgomi, K. Aschbacher, L. J. Crofford, and R. T. Faghih, "A system theoretic investigation of cortisol dysregulation in fibromyalgia patients with chronic fatigue," in 2019 41st Annual International Conference of the IEEE Engineering in Medicine and Biology Society (EMBC). IEEE, 2019, pp. 6896–6901.
- [39] D. R. Bach, G. Flandin, K. J. Friston, and R. J. Dolan, "PsPM-SCRV10: Skin conductance responses to loud sounds, simultanously recorded from palm, fingers and foot," Feb. 2017. [Online]. Available: https://doi.org/10.5281/zenodo.291465
- [40] D. R. Bach, G. Flandin, K. J. Friston, and R. J. Dolan, "PsPM-SCRV5: Skin conductance responses to auditory oddballs," Feb. 2017. [Online]. Available: https://doi.org/10.5281/zenodo.291445
- [41] D. R. Bach, G. Flandin, K. J. Friston, and R. J. Dolan, "PsPM-SCRV6: Skin conductance responses to pain by electric stimulation," Feb. 2017. [Online]. Available: https://doi.org/10.5281/zenodo.291446
- [42] D. R. Bach, G. Flandin, K. J. Friston, and R. J. Dolan, "PsPM-SCRV7: Skin conductance responses to white noise sounds in quick succession," Feb. 2017. [Online]. Available: https://doi.org/10.5281/zenodo.291448
- [43] D. R. Bach, G. Flandin, K. J. Friston, and R. J. Dolan, "PsPM-SCRV9: Skin conductance responses to visual targets," Feb. 2017. [Online]. Available: https://doi.org/10.5281/zenodo.291449
- [44] D. R. Bach, G. Flandin, K. J. Friston, and R. J. Dolan, "Modelling event-related skin conductance responses," *International Journal of Psychophysiology*, vol. 75, no. 3, pp. 349–356, 2010.
- [45] H. Prautzsch, W. Boehm, and M. Paluszny, Bézier and B-spline techniques. Springer Science & Business Media, 2013.
- [46] D. R. Bach, K. J. Friston, and R. J. Dolan, "An improved algorithm for model-based analysis of evoked skin conductance responses," *Biological* psychology, vol. 94, no. 3, pp. 490–497, 2013.
- [47] Z. Ghasemi, J. C. Lee, C.-S. Kim, H.-M. Cheng, S.-H. Sung, C.-H. Chen, R. Mukkamala, and J.-O. Hahn, "Estimation of cardiovascular risk predictors from non-invasively measured diametric pulse volume waveforms via multiple measurement information fusion," *Scientific reports*, vol. 8, no. 1, pp. 1–11, 2018.
- [48] J. F. Murray, "Visual recognition, inference and coding using learned sparse overcomplete representations," Ph.D. dissertation, University of California, San Diego, 2005.
- [49] G. H. Golub, M. Heath, and G. Wahba, "Generalized cross-validation as a method for choosing a good ridge parameter," *Technometrics*, vol. 21, no. 2, pp. 215–223, 1979.
- [50] R. Zdunek and A. Cichocki, "Improved m-focuss algorithm with overlapping blocks for locally smooth sparse signals," *IEEE Transactions on Signal Processing*, vol. 56, no. 10, pp. 4752–4761, 2008.
- [51] N. A. Macmillan and C. D. Creelman, Detection theory: A user's guide. Psychology press, 2004.
- [52] C. S. Moskowitz and M. S. Pepe, "Quantifying and comparing the predictive accuracy of continuous prognostic factors for binary outcomes," *Biostatistics*, vol. 5, no. 1, pp. 113–127, 2004.
- [53] V. G. Macefield and B. G. Wallin, "The discharge behaviour of single sympathetic neurones supplying human sweat glands," *Journal of the* autonomic nervous system, vol. 61, no. 3, pp. 277–286, 1996.

[54] D. R. Bach, G. Castegnetti, C. W. Korn, S. Gerster, F. Melinscak, and T. Moser, "Psychophysiological modeling: Current state and future directions," *Psychophysiology*, vol. 55, no. 11, p. e13214, 2018.

- [55] D. S. Wickramasuriya and R. T. Faghih, "A marked point process filtering approach for tracking sympathetic arousal from skin conductance," *IEEE Access*, 2020.
- [56] D. Wickramasuriya and R. T. Faghih, "A novel filter for tracking real-world cognitive stress using multi-timescale point process observations," in Engineering in Medicine and Biology Society (EMBC), 2019 41st Annual International Conference of the IEEE.
- [57] D. Wickramasuriya and R. T. Faghih, "A cortisol-based energy decoder for investigation of fatigue in hypercortisolism," in Engineering in Medicine and Biology Society (EMBC), 2019 41st Annual International Conference of the IEEE.
- [58] D. S. Wickramasuriya and R. T. Faghih, "Online and offline anger detection via electromyography analysis." in 2017 IEEE Healthcare Innovations and Point of Care Technologies (HI-POCT).
- [59] D. S. Wickramasuriya and R. Faghih, "A mixed-filter algorithm for arousal tracking from galvanic skin response and heart rate measurements." in *IEEE-EMBS Iternational Conference on Biomedical and Health Informatics*, May 2019.
- [60] M. B. Ahmadi, A. Craik, H. F. Azgomi, C.-V. J. L. Francis, J. T., and R. T. Faghih, "Real-time seizure state tracking using two channels: A mixed-filter approach," in 2019 53rd Asilomar Conference on Signals, Systems, and Computers.
- [61] A. S. Ravindran, S. Nakagome, D. S. Wickramasuriya, J. L. Contreras-Vidal, and R. T. Faghih, "Emotion recognition by point process characterization of heartbeat dynamics." in 2019 IEEE Healthcare Innovations and Point of Care Technologies (HI-POCT).
- [62] H. Fekri Azgomi, D. S. Wickramasuriya, and R. T. Faghih, "State-space modeling and fuzzy feedback control of cognitive stress," in 41st Annual International Conference of the Engineering in Medicine and Biology Society (EMBC). IEEE, July 2019.
- [63] H. Fekri Azgomi and R. T. Faghih, "A wearable brain machine interface architecture for regulation of energy in hypercortisolism," in *IEEE Asilomar Conference on Signals, Systems, and Computers*. IEEE, November 2019.
- [64] R. T. Faghih, M. A. Dahleh, and E. N. Brown, "An optimization formulation for characterization of pulsatile cortisol secretion," *Frontiers in neuroscience*, vol. 9, p. 228, 2015.
- [65] M. Seet, M. R. Amin, N. I. Abbasi, J. Hamano, A. Bezerianos, R. T. Faghih, N. Thakor, and A. Dragomir, "Olfactory-induced positive affect and autonomous response as a function of hedonic and intensity attributes of fragrances," in *Engineering in Medicine and Biology Society* (EMBC), 2020 42nd Annual International Conference of the IEEE.